

D2.4 - Protocols for SEI composition prediction

VERSION

VERSION	DATE
1	27/2-2024

PROJECT INFORMATION

GRANT AGREEMENT NUMBER	957189
PROJECT FULL TITLE	Battery Interface Genome - Materials Acceleration Platform
PROJECT ACRONYM	BIG-MAP
START DATE OF THE PROJECT	2020-09-01
DURATION	3 years
CALL IDENTIFIER	H2020-LC-BAT-2020-3
PROJECT WEBSITE	big-map.eu

DELIVERABLE INFORMATION

WP NO.	2
WP LEADER	UU
LEAD BENEFICIARY	CTH
CONTRIBUTING PARTNERS	WWU, FZJ, 3DS
NATURE	Report
AUTHORS	Soniya Rao (SR) and Patrik Johansson (PJ), CTH.
CONTRIBUTORS	Vignesh Thangavel (CTH), Zaher Slim (CTH)
CONTRACTUAL DEADLINE	29/2-2024
DELIVERY DATE TO EC	28/2-2024
DISSEMINATION LEVEL (PU/CO)	PU

ACKNOWLEDGMENT



This project has received funding from the European Union's Horizon 2020 research and innovation programme under grant agreement No 957189. The project is part of BATTERY 2030+, the large-scale European research initiative for inventing the sustainable batteries of the future.



ABSTRACT

This report summarizes the different protocols designed, developed, and used within WP2 of BIG-MAP to predict the SEI-formation. The methods applied stretch from DFT to molecules via configurations sampled from MD simulations to statistical mechanics. This enables us to, mostly at a proof-of-concept level, target several important features and phenomena: *i)* the initial reduction reaction potentials of special additives as well as salt anions, *ii)* the reduction reactions and products of lithium ion-containing solvates, foremost the organic solvent reduction, and *iii)* the solubilities of prospective SEI-components, focusing on small inorganic species. All of these protocols are useful both in their own right and as verification tools for other modelling approaches and to further explain experimental observations.

TABLE OF CONTENTS

1. CONTEXT OF D2.4	3
2. PROTOCOL #1 - PREDICTING REDUCTION OF SEI-FORMING ADDITIVES	4
2.1 SIMULATION PROTOCOL - DFT	4
2.2 RESULTS: REDUCTION POTENTIALS OF SEI-FORMING ADDITIVES	5
3. PROTOCOL #2 – PREDICTING SOLVATE REDUCTION PATHWAYS AND PRODUCTS	7
3.1 SIMULATION PROTOCOL – MD+DFT	7
3.2 RESULTS: RELATIVE STABILITIES AND REACTION PATHWAYS	8
4. PROTOCOL #3 - PREDICTING PROSPECTIVE SEI COMPONENTS' SOLUBILITY	13
4.1 SIMULATION PROTOCOL – DFT+COSMO-RS	13
4.2 RESULTS: SOLUBILITY OF INORGANIC SEI SALTS	16
4.2.1 MODEL VALIDATION - SOLUBILITY IN WATER	16
4.2.2 SOLUBILITY IN DMC AND PC	17
5. SUMMARY	18
6. REFERENCES	19

1. Context of deliverable 2.4

The nature and stability of the interfaces between the electrolyte and the two electrodes are crucial for lithium-ion batteries' stable and long-term operation. In particular, the solid electrolyte interphase (SEI) layer developing at the anode during the very formation stages of a battery cell's life is of uttermost importance as it prevents continuous electrolyte consumption at the low electrochemical potentials existing at, for example, graphite anodes, close to 0 V vs. Li^+/Li .

Most often, the SEI (as well as the cathode electrolyte interphase – the CEI) is studied experimentally and most often from an electrode and solid-state perspective, e.g., surface analysis by XPS and/or SEM. However, as the SEI initially and fundamentally develops from the electrolyte degrading, another perspective may be rewarding, i.e., that of the electrolyte. This is not the least true from a computational point of view. The model systems can be made discretely molecular rather than extended periodic solids, hence more suited for fast screening efforts and mapping of chemical space. These model systems and approaches can then target various electrolyte components, such as salts and solvents, in a wide sense but can also especially focus, e.g., on the electrolyte additives used to create better / more stable SEIs, known as SEI-formers.

In BIG-MAP WP2, we have devised, developed, and validated three protocols to be used to predict SEI composition in “detail” by modelling from an electrolyte point of view. The first predicts the electrochemical potentials at which electrolyte components, especially various SEI-formers, are reduced. This thus mimics the experimental situation of the pre-cycling made during the formation stage but only takes into account the very initial reduction reaction without actually looking at the SEI formed as such. This is a relatively straightforward approach, and the protocol is well-developed.

The second protocol uniquely targets the charge carrier of interest, the lithium cation dissolved by the electrolyte solvent, and in particular, how the various parts of these lithium cation-containing solvates may reductively react at/close to the anode surface. The focus is here on the degradation of the ethylene carbonate (EC) solvent known to occur and the possible pathways and products resulting from these, including the energetics and barriers involved. This is a much less explored area, with many degrees of freedom, and the protocol must instead be seen as a proof-of-concept to be further validated by other experimental or computational approaches.

The third and final protocol takes the stance that regardless of what the product of any electrolyte reduction process is, it must not be very soluble in the electrolyte if it is to be part of the SEI formed. This is a very novel approach to model SEIs, which demands a - to the field - relatively new set of computational tools to be applied and the approach to be validated by model systems. The protocol and approach also hold the complexity of moving from molecular local discrete models to a global property (solubility), which means that quantitative results may be beyond reach. The focus is thus on the semi-quantitative level

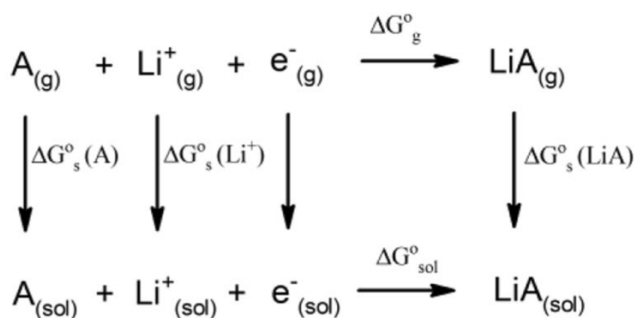
and, not the least, the qualitative level to bring further understanding of both real results and further needs/possibilities of protocol development.

Combined, the three protocols give direct computational predictive support to both experimental and other computational efforts, and they also challenge the perspective of how we, by modelling (can) target the SEI composition origins and thereby adds both fundamental understanding as well as battery development support.

2. Protocol #1 - predicting a reduction of SEI-forming additives

2.1 Simulation protocol - DFT

A methodological benchmark here attacks SEI-forming additives, and the protocol adopted originates from several computational approaches and methods tested to predict and describe additive properties.^[1] As a result of the analysis of ten SEI-forming compounds, the methodology based on the simultaneous reduction of the lithium cation and its coordination to ensure, if needed, electroneutrality with the solvent/additive yielded the best results close to experimental values. The thermodynamic path shown in Scheme 1 has been considered the most efficient to predict the reduction behavior. A correction of -1.46 V was used to convert absolute potentials to the Li^+/Li^0 scale.^[2] For any accurate prediction, an implicit solvent was found to be necessary, but the exact solvent permeability (ϵ) was not a crucial factor as long as $\epsilon > 20$. Thus, being the best-parameterized solvent for implicit solvent models, water can be used as a decent approximation for all additives with $\epsilon > 20$. A comparison of different methods and basis sets revealed that the functional M06-2X was the most effective for describing the reduction potential compared to other functionals.^[3-6] The popular 6-311++G** basis set^[7,8] gave quite good results compared to other larger and more advanced basis sets; only the Dunning basis set, aug-cc-pVTZ,^[9] provided data in better agreement with the experimental data. The Dunning basis set is, however, computationally much more expensive. It uses 46 basis functions for each first-row atom, while all other basis sets comprise only 22–24 basis functions. Hence, due to its combination of accuracy and efficiency, we chose the Pople basis set 6-311++G(d,p) for subsequent use.^[1] An analysis of other popular descriptors revealed that it is impossible to assess the reduction potential based on simple parameters such as the LUMO energy in a wide range of chemical compounds; such screening can be useful for screening compounds with only small differences in their chemical structure.

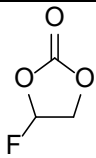
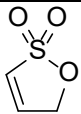
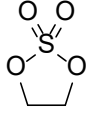
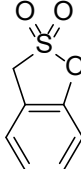
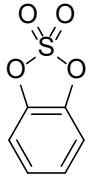
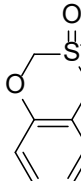


Scheme 1. Thermodynamic paths are implemented to calculate redox potentials for an additive A or a salt LiA. (The energy difference from vacuum to solution for an electron is very small; here defined = 0).

2.2 Results: Reduction potentials of SEI-forming additives

Reduction potential studies have been focused on BIG-MAP-relevant conducting salts and functional additives considered in WP4, WP5, and WP6. Depending on the obtained results and level of electrolyte formulation enhancement reported in D6.1, certain conducting salts have been selected as feeding units for HT (high throughput) assays and also for their beneficial film-forming ability (LiBOB and LiDFOB) or their moisture/impurity scavenging ability (LiTDI, LiPDI and LiHDI). At WUT, the formulations that involved synthesizing 5-membered-ring molecules (DTD, DTDPH, and DCKEA) and other additives previously reported in D6.1 have been selected as potential candidates to implement the simulation protocol (Table 1). The thermodynamic path shown in Scheme 1 was used to calculate the absolute reduction potential of the additives provided in Table 2.

Table 1. Selected SEI-forming additives and film-forming/scavenging lithium salts.

Structure	Name	Acronym	Structure	Name	Acronym
	Fluoroethylene carbonate	FEC		1,3-Propene sultone	PES
	1,3,2-Dioxathiolane 2,2-dioxide	DTD		3H-1,2-Benzoxathiole 2,2-dioxide	PSPH
	1,3,2-Benzodioxathiole 2,2-dioxide	DTDPH		1,4,2-Benzodioxathiine 2,2-dioxide	PSOPH



	Dicyanoketene ethylene acetal	DCKEA		<i>N,O</i> -Bis(trimethylsilyl)-acetamide	BSA
	Vinylene carbonate	VC		Succinic anhydride	SA
	Propane sultone	PS		Triphenylphosphine oxide	TPPO
Selected lithium salts as electrolyte solutes					
	Lithium 4,5-dicyano-2-(trifluoromethyl)imidazole	LiTDI		Lithium 4,5-dicyano-2-(pentafluoroethyl)imidazole	LiPDI
	Lithium 4,5-dicyano-2-(heptafluoropropyl)imidazole	LiHDI		Lithium bis(oxalato)borate	LiBOB
	Lithium difluoro(oxalato)borate	LiDFOB			

Table 2. Reduction potentials using Scheme 1 and M06-2X/ 6-311++G(d,p) vs. $\text{Li}^+/\text{Li}^\circ$.

Additive	Experimental [V]	Calculated [V]	Difference [V]
BSA		-0.05	
DCKEA		1.75	
DTDPh	1.04 ^[16]	0.39	-0.65
DTD*	2.13 ^[14]	2.28	+0.15
FEC*	0.70 ^[10]	0.69	-0.01
PES	1.12 ^[16]	0.91	-0.21
PSOPh	0.85 ^[16]	3.56	+2.71
PSPh		0.33	
PS	(0.74 ^[16]), 1.75 ^[16]	1.90	(1.16) +0.15
SA		1.23	
TPPO		3.11	
VC*	1.40 ^[15]	1.11	-0.29
BOB	1.7 ^[11]	1.73	+0.03

DFOB	1.5 ^[12] , 1.4 ^[13]	1.38	-0.12, -0.02
HDI		1.20	
PDI		1.01	

From the results for the SEI-formers and salt anions, several conclusions can be made with respect to the protocol's predictive power. First, overall, we have a protocol readily available that, for many SEI-forming additives and popular anions, predicts their reduction potential to be ca. within +/- 0.2-0.3 V. We would like to stress that this is approximately the experimental accuracy of 0.1-0.2 V, which comes from the fact that it is not apparent where and how to precisely set the on-set of reduction, nor under what conditions the reduction potential is to be experimentally determined – no standard exists.

Second, as the protocol indeed does not contain either the electrolyte composition or any anode surface, which makes it very versatile and fast, it can, on the other hand, not be expected to catch any specific chemical reactions that may interfere. This may explain the much larger discrepancies in reduction potentials found for both DTDPH and PSOPH additives – and notably, these both contain a phenyl group and are also the only additives/species that do. Thus, this feature seems to bring a problem.

Third, there is also variety in the experimental values, both in accuracy and absolute numbers, which adds complexity and uncertainty alongside the limited number of species targeted for any statistics. This is, however, something that can, at least partially, be solved by incorporating the protocol, after further development, in pipelines involving high-throughput screening in future efforts.

Fourth and final, we have not ascertained why or whether special chemistries, such as the phenyl-containing species, may be harder for the protocol to handle or not or whether it is, e.g., a DFT functional or basis set issue. This is because many SEI-formers build on somewhat similar chemistries, but on the other hand, the protocol seems to handle both neutral and negatively charged species equally well.

3. Protocol #2 – predicting solvate reduction pathways and products

3.1 Simulation protocol – MD+DFT

One of the goals of WP2 was to develop stable and generic atomistic and QM methodologies that are usable for validating ML approaches. These are for some properties preferably created by combining different computational approaches to, in synergy, solve difficult problems, such as those stretching across different time and length scales – or even in the protocol input and output paths. Here, we devise a protocol that first utilizes MD

simulations made by WWU to feed structures (input) into DFT calculations performed at CTH that generate pathways and energetics (output). This is done first to obtain “realistic” lithium cation solvate structures and then assess these solvates’ relative thermodynamic stabilities and their stabilities vs. reduction reaction. As a proof-of-concept, we use “cut-outs” from the MD simulation trajectories to obtain the first solvation shell cation-solvent structures/complexes to target only the local structure around the Li^+ cation, which provides an idea of preferential solvation and, at the exact time sampling beyond what would be feasible using only DFT directly. As a very first approximation, only $[\text{Li}(\text{EC})_6]^{+1}$ type “cut-outs” were considered (Figure 1). The choice of EC as a single solvent is based on the fact that it is a common component in almost any LIB electrolytes and a common contributor to SEI formation. Still, it is not fully understood exactly how it contributes.

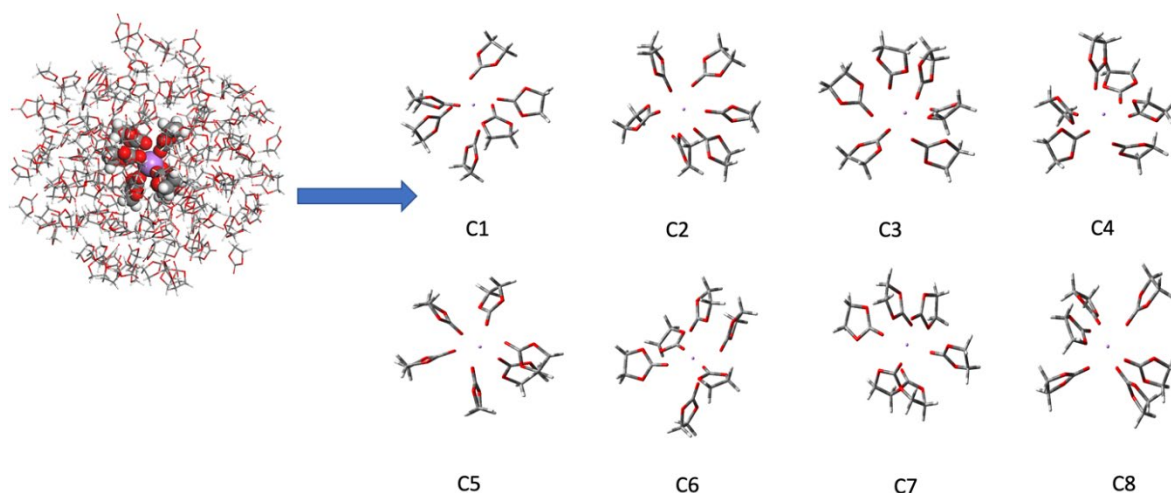


Figure 1. An MD simulation cell snapshot (left), with a single lithium-ion environment highlighted, and the eight different solvation structure “cut-outs” C1-C8 (right), each with a single lithium central atom and 6 EC solvent ligands (not necessarily all coordinating the lithium) – the starting geometries for the DFT calculations.

As a testbed for the proof-of-concept protocol development, each of the cut-outs C1-C8 shown in Figure 1 was, to study the solvation structure in more detail and, in particular, the EC solvent reductive decomposition reactions, subsequently transferred to full DFT geometry optimization (M06-2X/6-311+G(d,p)) in vacuum, rendering the structures and energies provided in Figure 2 and Table 3 below. While these might not resemble “real” structures, they show a proof-of-concept way of sampling a variety of structures. The way these structures are optimized can be fine-tuned by either explicit (2nd solvent shell included) or implicit (by SCRF, etc.) solvent also had. Still, the computational cost increases significantly, especially for the former approach.

3.2 Results: Relative stabilities and reaction pathways

In this results section, we will discuss in detail the relative stabilities and pathways relating to Figure 2 and Table 3.

Starting with a very general structural observation, we find that for the EC solvent, the carbonyl, i.e., C=O, bonds of the lithium-ion coordinated EC become slightly elongated (by ca. 0.03 Å), likely due to the polarizing power of the chemically complex lithium cation, while, likely as a secondary effect of this, the ether C-O bonds in the ring of the EC conversely contract (by ca. 0.04 Å). All with reference to the uncoordinated/“free” EC. This may seem like a detail, but it may be decisive with respect to (reduction) reaction dynamics. If so, other battery technologies, such as sodium-ion and/or potassium-ion batteries, may have quite different characteristics with respect to this property. Also, please note that while we designate all structures C1-C8 as $[\text{Li}(\text{EC})_6]^{+1}$, they do not all have the same coordination number (CN), nor is CN=6 dominant, and this is a more realistic view coming from the use of MD trajectory structure cut-outs rather than symmetrical/optimized DFT limited configurations.

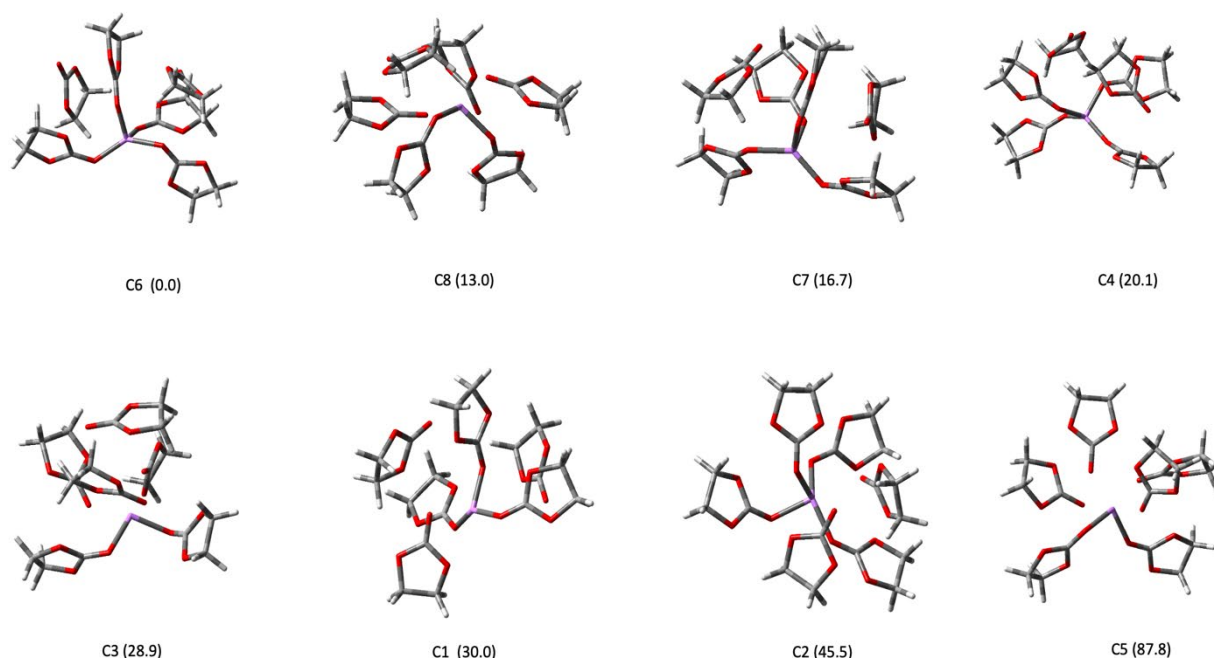


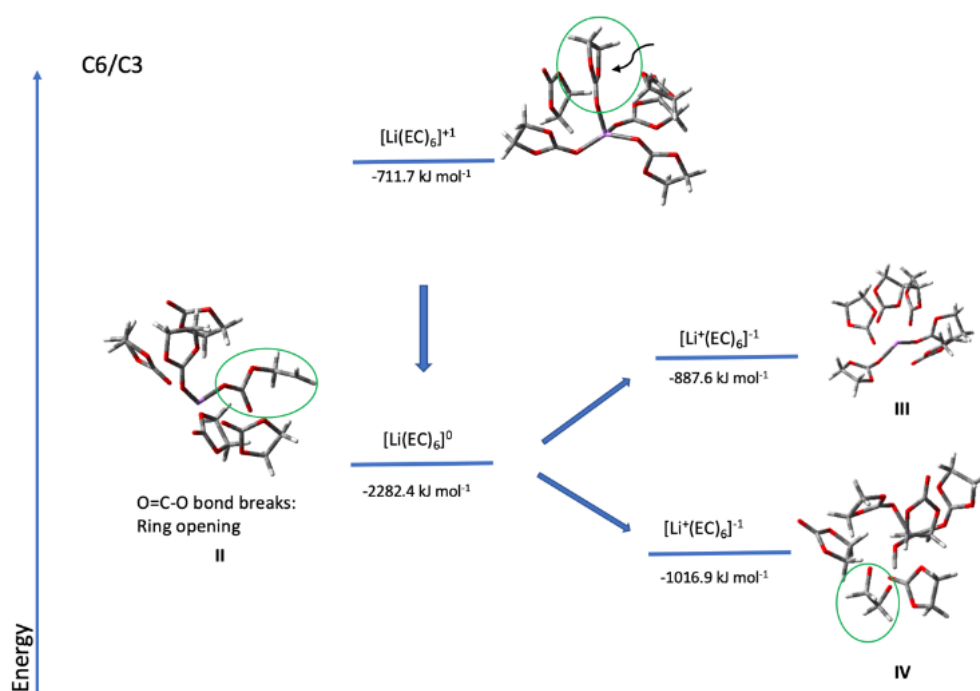
Figure 2. Optimized structures of $[\text{Li}(\text{EC})_6]^{+1}$ cut-outs C1-C8 at the M06-2X/6-311+G(d,p) level with the relative energies E_{rel} [kJ mol^{-1}] with respect to the lowest-energy structure (C6) within parenthesis.

Looking at the (EC) solvent decomposition reactions in general, these are more or less always presumed to result either from one- or two-electron reduction mechanisms – which in Table 3 is represented simply as providing one or two extra electrons to the optimized structures and after that calculating the single-point energies of the $[\text{Li}(\text{EC})_6]^0$ and $[\text{Li}(\text{EC})_6]^{-1}$ solvates, respectively. The underlying assumption is that the electron transfer and acceptance are so fast that no structural re-arrangement occurs in the same time frame. However, it should be noted that the exact energy differences likely are much too large, as we are handling reaction paths in vacuum, but they can be used semi-quantitatively.

Table 3. Relative (E_{rel}) and binding energies (ΔE) in kJ mol^{-1} at M06-2x/6-311+G(d,p) in vacuum.

	E_{rel} (kJ mol^{-1})	ΔE (kJ mol^{-1})		
		$(\text{Li}(\text{EC})_6)^{+1}$	$(\text{Li}(\text{EC})_6)^0$	$(\text{Li}(\text{EC})_6)^{-1}$
C6	0 (def)	-712	-2282	-1017
C8	+13	-699	-	-854
C7	+16.7	-695	-	-
C4	+20.1	-692	-896	-1094
C3	+28.9	-685	-2288	-878
C1	+30.0	-682	-902	-1243
C2	+45.5	-669	-896	-
C5	+87.8	-632	-966	-883

The relative energies presented do not provide much more information than that not all of C1-C8 belong to the same part of the potential energy surface. If they had, they would have been closer in energy after the DFT geometry optimization step – and the sampling would have been flawed. The binding energies, on the other hand, tell quite a bit about how the various structures can accommodate one or two extra electrons. Hence, e.g., C3 and C6 seem remarkably well-prepared to handle one additional electron, while C1 handles two better. This is all in a simplistic, energetic fashion, but below is the real unique outcome of the protocol, i.e., the pathways followed and the resulting products are outlined for a few examples. In principle, three main reduction reaction pathways have been deciphered (Figure 3).



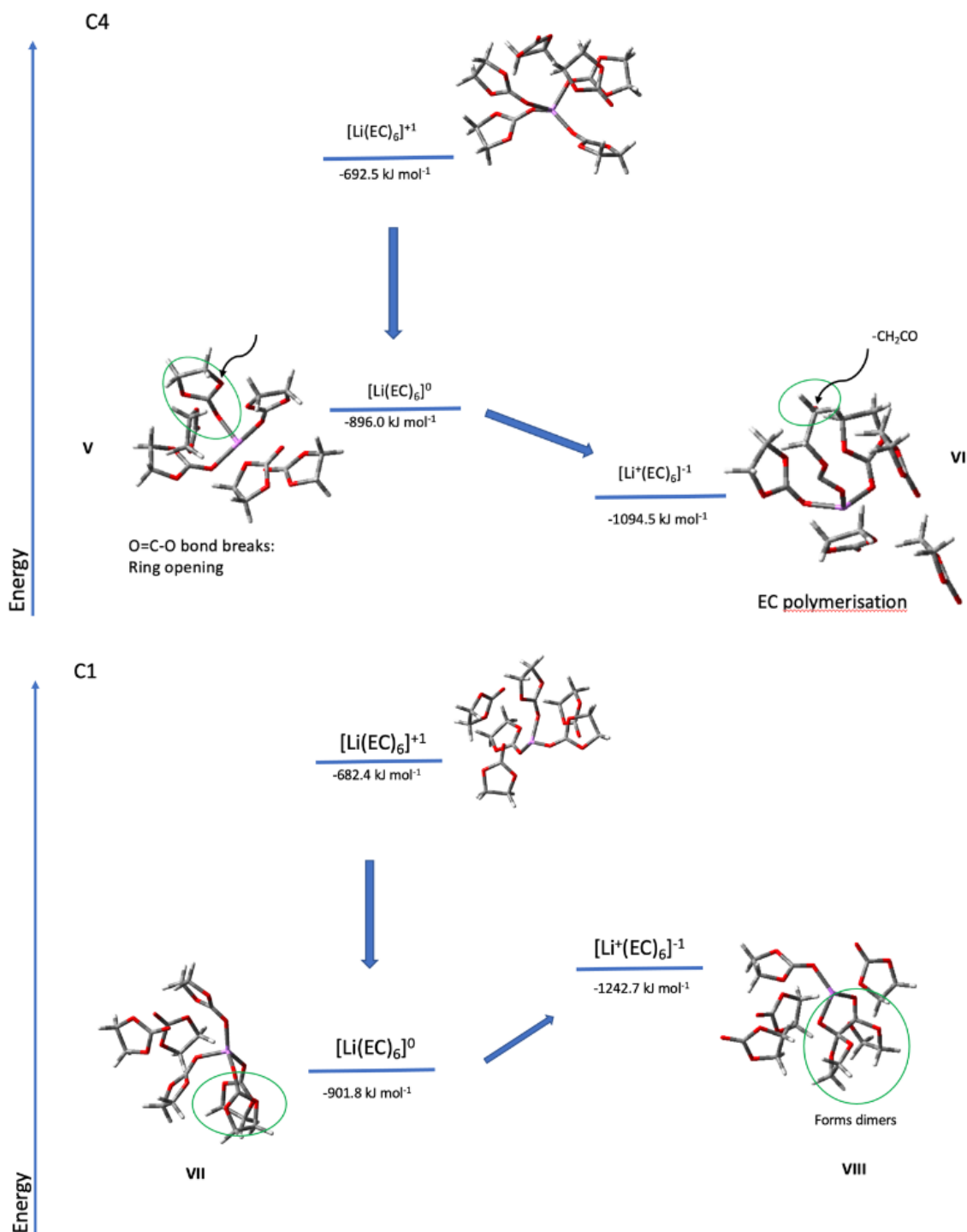


Figure 3. Pathways #1 and #2 (top and middle) for C6, and C3 and C4, respectively, all with homolytic ring-opening reactions, and Pathway #3 (bottom) for C1, with a final dimerization reaction to the right.



Looking at the eight solvates, C6, C3, C4, and C1 all undergo either homolytic ring opening or dimerization reactions, while C2, C5, C7, and C8 only do a local structure reorganization. Thus, we naturally focus on the former, and there are, in principle, three main pathways observed, which we describe to some extent below.

Pathway #1, for both C6 and C3 (Figure 3 top), the initial EC ring opening reduction reaction occurs via etherC-etherO (C-O) bond breaking and formation of a radical, anionic species **II**. Further reduction of **II** leads to the formation of CH₂O-CH₂O alongside solvated species containing Li oxycarbides (Li-O=C), or Li coordinated to two EC solvent molecules and additional free ECs (**IV**), OR a branch with a “simple” reorganization of **II** towards solvated clusters (**III**), also this with a Li coordinated to two EC solvent molecules.

C4 follows Pathway #2, with a slightly different ring opening reaction. Here the homolytic cleavage of the EC ring occurs via etherO – CH₂ bond breaking (CO-CH₂) (Figure 3 middle), and for this to occur, Li must be/is moved towards a bidentate coordination to one of the EC solvents and an elongation of the Li---C=O bond distances of ca. 0.12 Å is thereby obtained for all the coordinated EC solvent, as compared to the free solvents (**V**). The C=O bond close to the lithium cation shifts becomes quite elongated (1.583 Å) and weak and then undergoes further reduction, and finally, the ring-opening reaction is completed with the formation of radical anion: •OCCH₂CH₂OCOLi (lithium butyl carboxylate) (**VI**). From an SEI formation point-of-view, this anion radical may result in polymerization or radical dimerization reactions forming dicarbonates.

Finally, C1 and Pathway #3 are quite different as they begin with a reorganization from a CN=3 to a tetrahedral geometry (**VII**) (Fig. 3 bottom), which only after that, with an extra electron added, undergoes a ring dimerization reaction forming **VIII**.

Three possible reaction pathways for reducing the different C1-C8 [Li(EC)₆]⁺¹ cut-outs have been identified. The adiabatic reaction barrier heights are quite high, and it is likely safe to conclude that the lithium-coordinated EC solvents are those initially reduced by the electron transfer from the anode rather than the free EC solvents, pinpointing the role of the lithium-ion for the SEI formation. The role of, e.g., CNs and how/whether these affect the one-step electron reduction reactions or the homolytic ring opening remain unclear.

Of the three unique main pathways presented, two are one-electron reduction processes involving homolytic ring opening, which is the experimentally recognized reaction mechanism. Thermodynamically, the most favorable pathway is #2, followed by #3, and the least favorable is #1. It may be inferred from these results, and this is partly in line with the literature, that the part of an SEI that originates from solvent decomposition may mainly be comprised of lithium butylene carboxylate (CH₂CH₂OCOLi) and lithium ethylene carboxylate (CH₂OCOLi). However, the caveat for all pathways is that we consider only a single EC solvent electrolyte model system here, which either calls for very special experimental comparisons (as EC is a solid at room temperature) or careful computational comparisons. To develop this protocol further, more realistic electrolytes and/or more extensive sampling of structures may be needed. However, there is a large uncertainty as to how to assess

exactly how much more expansion of the data is needed to capture the most relevant structures and mechanisms for the solvent decomposition part of the SEI formation.

4. Protocol #3 - predicting prospective SEI components' solubility

4.1 Simulation protocol – DFT+COSMO-RS

While the former two protocols target the reduction reactions to predict the very formation stage of (prospective) SEI components, this protocol takes on to rather decide/predict whether the products of such reactions are soluble or not in the electrolyte – which affects their likelihood to either stay in the SEI after being formed or be dissolved and transported away and not take part in the SEI formation.

Overall, this protocol holds a computational strategy that combines local accurate ion-ion interactions via DFT calculations with thermodynamics in the shape of statistical mechanics via the conductor-like screening model for real solvents (COSMO-RS). Using this approach, we predict the solubilities of (prospective) SEI components and verify these vs. experimental data. The focus is here on the inorganic parts of the SEI, quite naturally on alkali. Li and alkali earth metals, the former to target the batteries at hand and the latter to evaluate the generality of the protocol, as well as to provide more data. The prime inorganic components in focus are carbonates, fluorides, etc. Still, the protocol is/can be expanded to other concepts and other types of SEI components, incl. organic species.

The thermal property data needed as input to the COSMO-RS calculations, i.e., the melting temperature (T_m) and the enthalpy of fusion (ΔH_{fus}), were mainly taken from the literature, complemented with a few selected salts, where data were extracted from differential scanning calorimetry (DSC) experiments (Table 4).

The very starting point for the protocol, leading up to the COSMO-RS calculations, is to first use DFT calculations to generate optimized geometries of all species to be studied, here ions and solvents, and subsequently create COSMO-files for each species, that contain the σ -surfaces of the species. For the DFT calculations, we employed the PB86 functional and the TZVP basis set, the initial geometry optimizations were carried out in the gas phase, and then the conductor-like self-consistent reaction field (SCRf) COSMO ($\epsilon=\infty$) was added to implicitly account for solvent effects. The subsequent COSMO-RS calculations used the BP_TZVP_21 parameterization in COSMOtherm, and the absolute solubilities were calculated using the solid-liquid equilibrium (SLE) method.

One intrinsic problem of COSMO-RS is that it handles hard cations, such as Li^+ and Mg^{2+} , but also small anions, such as F^- , less favorably due to their high polarization charge densities and thereby narrow σ -profiles (Figure 4), leading to problems not the least for solubility calculations. A remedy to this, and the strategy we employ herein, is to use explicitly



solvated ions. The so-created solvates have much broader σ -profiles; see, e.g., the example of $[\text{Li}(\text{S})_4]^+$ for $\text{S} = \text{H}_2\text{O}$ or PC in Figure 4, that most often are in the range of the σ -profiles of the electrolyte solvents employed. Indeed, without using the approach of explicit solvation via solvates, no solubilities were possible to calculate for, e.g., LiF and CaF_2 .

The salt solubilities (x or X) are subsequently calculated using: $x_i^{bs} = \frac{x_i^{ss}}{1+n_s x_i^{ss}}$, where x_i^{bs} and x_i^{ss} are the mole fractions of the “bare” ions and solvates, respectively, and n_s is the number of solvent molecules in the cationic and anionic solvates (see Table 4).

Table 4. SEI components targeted and selected experimental and computational properties.

Species	T_m (°C)	ΔH_{fus} (kJ/mol)	n_s cationic solvate	n_s anionic solvate	Solvent	Solubility (mole fraction)	
						Exp.	Comp.
Li ₂ CO ₃	732	44.8	8 (2x4)	0	H ₂ O (25 °C)	3.15x10 ⁻³	2.00x10 ⁻²
					DMC (20 °C)	1.03x10 ⁻⁴	2.23x10 ⁻³
					PC (20 °C)	2.19x10 ⁻⁴	4.20x10 ⁻³
LiCl	610	19.8	4	0	H ₂ O (25 °C)	2.64x10 ⁻¹	4.51x10 ⁻²
					DMC (25 °C)	1.03x10 ⁻⁴	2.28x10 ⁻²
					PC (25 °C)	8.22x10 ⁻⁴	3.18x10 ⁻²
LiC ₂ H ₅ O	201	7.0	4	0	H ₂ O (25 °C)		3.88x10 ⁻¹
					DMC (20 °C)	5.53x10 ⁻⁴	4.15x10 ⁻¹
					PC (20 °C)	2.88x10 ⁻⁵	4.10x10 ⁻¹
LiF	848.2	27.1	4	1	H ₂ O (25 °C)	9.31x10 ⁻⁴	4.39x10 ⁻³
					DMC (25 °C)	1.07x10 ⁻⁵	5.46x10 ⁻³
					DMC (20 °C)	1.85x10 ⁻³	4.86x10 ⁻³
					PC (25 °C)	4.56x10 ⁻⁴	8.35x10 ⁻³
LiOH	473	20.9	4	0	H ₂ O (25 °C)	8.59x10 ⁻²	7.02x10 ⁻²
					DMC (20 °C)	2.09x10 ⁻³	2.80x10 ⁻²
					PC (20 °C)	1.76x10 ⁻⁴	3.27x10 ⁻²
LiNO ₃	253	26.7	4	0	H ₂ O (25 °C)	2.14x10 ⁻¹	6.67x10 ⁻²
					DMC (25 °C)	2.06x10 ⁻⁴	3.01x10 ⁻¹
					PC (25 °C)	1.41x10 ⁻²	4.22x10 ⁻²
Na ₂ CO ₃	856	29.7	8 (2x4)	0	H ₂ O (25 °C)	4.96x10 ⁻²	4.40x10 ⁻²
					DMC (25 °C)		8.02x10 ⁻³
					PC (25 °C)		1.88x10 ⁻²
NaC ₂ H ₅ O	320	46.3	4	0	H ₂ O (25 °C)	3.11x10 ⁻¹	4.63x10 ⁻⁴
					DMC (25 °C)		1.83x10 ⁻³
					PC (25 °C)		3.24x10 ⁻³
NaF	996	33.4	4	1	H ₂ O (25 °C)	1.74x10 ⁻²	2.12x10 ⁻³



					DMC (25 °C)		1.44×10^{-3}
					PC (25 °C)		2.90×10^{-3}
NaHCOO	259	15.0	4	0	H ₂ O (18 °C)	8.92×10^{-1}	9.35×10^{-2}
					DMC (25 °C)		8.69×10^{-2}
					PC (25 °C)		9.59×10^{-2}
NaOH	323	6.6	4	0	H ₂ O (25 °C)	3.11×10^{-1}	1.59×10^{-1}
					DMC (25 °C)		1.52×10^{-1}
					PC (25 °C)		1.47×10^{-1}
CaCO ₃	1339	53	4	0	H ₂ O (25 °C)	2.34×10^{-6}	6.00×10^{-8}
					DMC (25 °C)		1.88×10^{-12}
					PC (25 °C)		6.22×10^{-6}
CaF ₂	1418	30.0	4	2	H ₂ O (25 °C)	3.69×10^{-6}	4.32×10^{-5}
					DMC (25 °C)		2.67×10^{-6}
					PC (25 °C)		3.12×10^{-3}
MgCO ₃	990	59.0	4	0	H ₂ O (25 °C)	1.28×10^{-4}	1.19×10^{-6}
					DMC (25 °C)		7.87×10^{-13}
					PC (25 °C)		4.57×10^{-6}
MgF ₂	1236	58.7	4	2	H ₂ O (25 °C)	3.76×10^{-5}	4.05×10^{-6}
					DMC (25 °C)		8.61×10^{-8}
					PC (25 °C)		1.21×10^{-4}

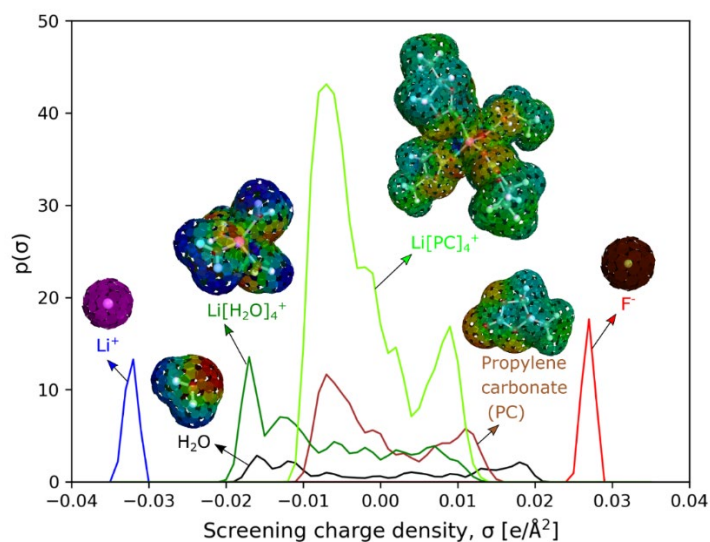


Figure 4. Examples of σ -profiles/surfaces of ions, solvents, and solvates relevant for LIB SEIs.

4.2 Results: Solubility of inorganic SEI salts

First, a comparison between calculated and experimental solubilities is made for water salts to validate the method. We focus firsthand on qualitative differences, deciphering *why* there are deviations, and secondly on semi-quantitative agreement, using the root mean square deviation (RMSD) as the single quantitative measure of *how large* the deviations are, complemented by simple and intuitive visualization. This is made for lithium salts only before finally showcasing calculated solubilities of all salts in DMC and PC vs. experimental values of salts in water.

4.2.1 Model validation - solubility in water

The solubility in water is readily available in the literature for all our salts (Table 4). Furthermore, much of the development of the computational approach used has been made with aqueous systems in mind. Overall, we find very good qualitative agreement for the SEI species of LIBs and SIBs, while for the multivalent cation-based species, and especially for CaCO_3 and MgCO_3 , there are much larger deviations (Fig. 5). One reason for the latter, as we have already remedied the hard cation/anion problem via explicit solvation, could be that long-range interactions are not considered in COSMO-RS and this may especially affect those salts where either one of or both the cations and anions are divalent. An additional problem is that no non-ideality of the electrolytes, such as the Debye–Hückel effect, is considered, which also might be more pronounced for divalent chemistries. We thus here have at least three difficult cases included: a) salts with both divalent cations and anions, b) salts with the CO_3^{2-} divalent anion, and c) salts with the F⁻ anion – which is a species challenging to treat correctly by DFT. While the resulting RMSD is 0.99, looking only at the monovalent (Li, Na) species (Fig. 5), the agreement is much better.

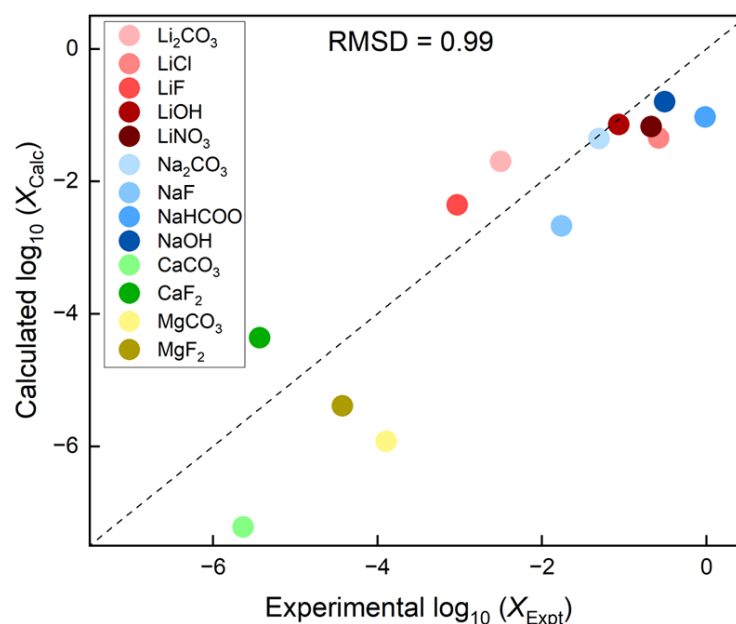


Figure 5. Calculated and experimental solubilities in water from Table 4.

4.2.2 Solubility in DMC and PC

The solubilities in non-aqueous solvents, such as DMC and PC, are reported only for a few lithium salts and not at all for Na, Mg, or Ca-salts. Starting with DMC as a solvent, there is notably a sizeable qualitative disagreement vs. experimental data (Fig. 6), where stark differences are observed for much of the data: LiF (25°C), LiCl, LiOH, and LiNO₃. One origin could be the low solubilities in DMC, due to its low permittivity, overall making predictions harder and notably overestimating the solubilities for all salts. Still, perhaps it is also due to less trustworthy experimental data to validate against – compared to the aqueous systems/water. The latter can be exemplified by the fact that the solubility of LiF in DMC can vary by no less than two orders of magnitude: 1.07×10^{-5} and 1.85×10^{-3} mole fractions, respectively. Quantitatively, the resulting RMSD (1.99) is significantly larger than for water as a solvent, but there are also much fewer data points, intrinsically leading to poor statistics.

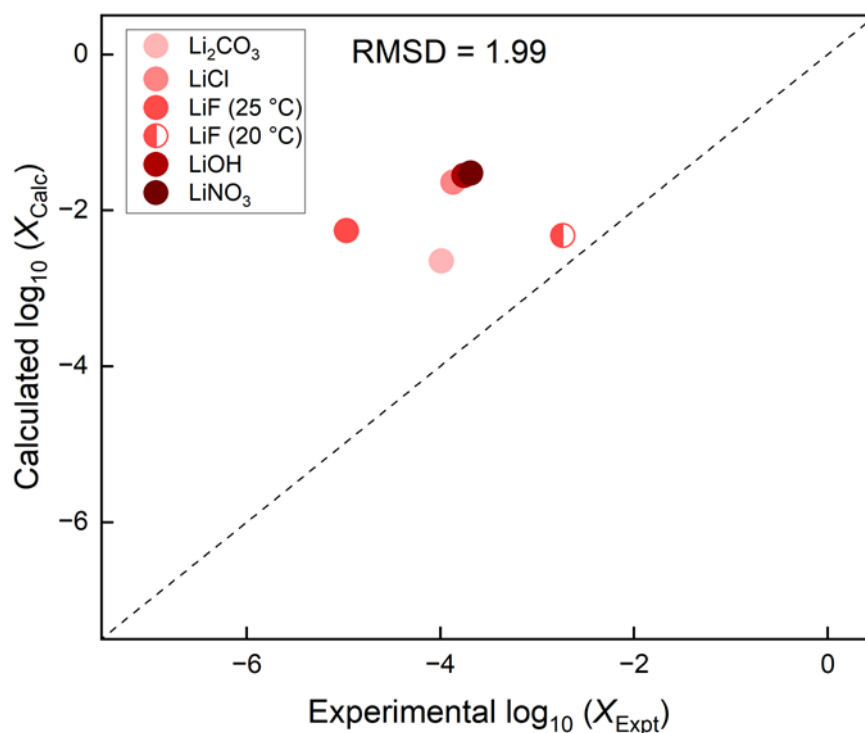


Figure 6. Experimental and calculated solubilities in DMC from Table 4.

Turning to PC as a solvent, the RMSD is intermediate (1.22), which largely is due to a general overestimation by slightly over one order of magnitude (Fig. 7), but the predicted solubilities do have a good qualitative agreement with the experimentally observed.

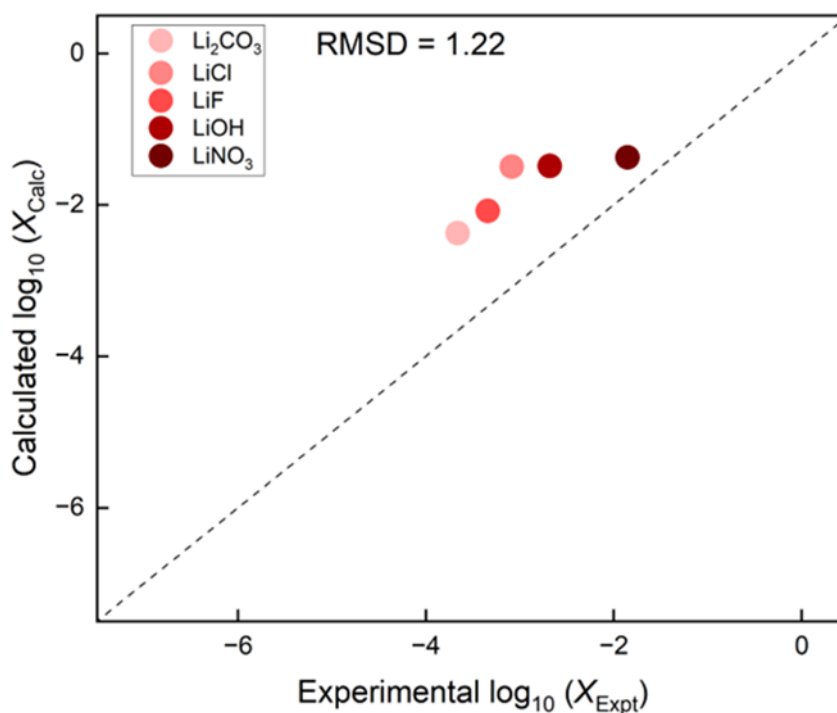


Figure 7. Experimental and calculated solubilities in PC from Table 4.

Overall and qualitatively, the trends in solubilities for the different salts are reminiscent of those in water. The protocol, based on a tailored COSMO-RS computational approach to predict the solubilities of SEI-components for a given electrolyte solvent, is highly efficient as the DFT calculations of the species are carried out only once and the resulting COSMO files can be reused in multiple fast COSMO-RS solubility calculations. Overall, the changes in solubility for our few selected solvents (H_2O , DMC, and PC) qualitatively, and sometimes even semi-quantitatively, follow the experimentally observed or expected trends. Some of the pronounced deviations could be due to the fact that the Debye–Hückel effect is not being considered in the COSMO-RS approach. In conclusion, the presented computational strategy could genuinely assist in designing more stable SEI layers through qualitative and semi-quantitative solubility predictions of any proposed SEI components.

5. Summary

Three different protocols have been devised using an electrolyte perspective on the SEI formation – with partially other targets, advantages, and problems. Common to them all is, however, that they use discrete molecular level models, with the promise to be moderately computationally expensive, and two of them also combine several computational methods in the protocols, MD+DFT and DFT+COSMO-RS, respectively. The protocols can indeed all be used in a predictive fashion: #1 is the most mature and quantitative, and for many species, gives predictions within experimental uncertainty for the reduction potentials; #2



focuses on ways to bring further understanding on possible reduction pathways and mechanism, while, *e.g.*, the energies and barriers likely carry only very little quantitative value; and #3 is intermediate as it semi-quantitatively addresses a global property by starting from minimal local models using DFT. While protocol #2 needs either a specially designed experiment to be validated or applied to a more complex and realistic electrolyte composition, protocols #1 and #3 can now be devised to create, *e.g.*, libraries as they are. The latter are already (partially) validated vs. experiments, which means that they also are/can be part of the toolbox needed to validate different AI/ML approaches to SEI formation.

6. References

1. P. Jankowski, W. Wieczorek, P. Johansson, *J. Mol. Model*, **2017**, 23, 6.
2. S. Trasatti, *Pure Appl. Chem.*, **1986**, 58, 955–966.
3. Y. Zhao, N.E. Schultz, D.G. Truhlar, *J. Chem Phys.*, **2005**, 123, 194101.
4. Y. Zhao, D.G. Truhlar, *Theor. Chem. Accounts*, **2008**, 120, 215–241.
5. R. Peverati, D.G. Truhlar, *J. Phys. Chem. Lett.*, **2011**, 2, 2810–2817.
6. R. Peverati, D.G. Truhlar, *Phys. Chem. Chem. Phys.*, **2012**, 10, 3171.
7. R. Krishnan, J. S. Binkley, R. Seeger, J. A. Pople, *J. Chem. Phys.*, **1980**, 72, 650–65.
8. T. Clark, J. Chandrasekhar, G.W. Spitznagel, P. V. R. Schleyer, *J. Comput Chem.*, **1980**, 4, 294–301.
9. R. A. Kendall, Jr. T. H. Dunning, R. J., Harrison, *J. Chem Phys.*, **1986**, 96, 6796–6806.
10. I. A. Profatilova, S. S. Kim, N. S. Choi, *Electrochim. Acta*, **2009**, 54, 4445–4450.
11. K. Xu, S. S. Zhang, U. Lee, J. L. Allen, T. R. Jow, T. R. Libob, *Journal of Power Sources* **2005**, 146, 79-85.
12. S. S. Zhang, *Electrochemistry Communications*, **2006**, 8, 1423-1428.
13. S. Lee, J. -G Han, Y. Lee, M.-H. Jeong, W. C. Shin, M. Ue, N.-S. Choi, *Electrochimica Acta*, **2014**, 137, 1-8.
14. P. Janssen, R. Schmitz, R. Muller, P. Isken, A. Lex-Balducci, C. Schreiner, M. Winter, I. Cekvic-Laskovic, R. Schmitz, *Power Sources*, **2004**, 125, 101–106.
15. X. Zhang, R. Kosteki, T. J. Richardson, J. K. Pugh, P.N. Ross, *J. Electrochem Soc.*, **2001**, 148, 1341–1345.
16. P. Jankowski, N. Lindahl, J. Weidow, W. Wieczorek, P. Johansson, *ACS Appl. Energy Mater.* **2018**, 1, 2582–2591.